

Gas-atomized particles of giant magnetocaloric compound HoB₂ for magnetic hydrogen liquefiers

Takafumi D. Yamamoto · Hiroyuki Takeya · Akiko T. Saito · Kensei Terashima ·
Pedro Baptista de Castro · Takenori Numazawa · Yoshihiko Takano

Received: date / Accepted: date

Abstract The processing of promising magnetocaloric materials into spheres is one of the important issues on developing high-performance magnetic refrigeration systems. In the present study, we achieved in producing spherical particles of a giant magnetocaloric compound HoB₂ by a crucible-free gas atomization process, despite its high melting point of 2350 °C. The particle size distribution ranges from 100 to 710 μm centered at 212-355 μm with the highest yield of 14-20wt% of total melted electrode, which is suitable for magnetic refrigeration systems. The majority of the resulting particles are mostly spherical with no contamination during the processing, while unique microstructures are observed on the surface and inside. These spherical particles exhibit sharp magnetic transitions and huge magnetic entropy change of 0.34 J cm⁻³ K⁻¹ for a magnetic field change of 5 T at 15.5 K. The high sphericity and the high magnetocaloric performance suggest that the HoB₂ gas-atomized particles have good potential as magnetic refrigerants for use in magnetic refrigerators for hydrogen liquefaction.

Keywords Magnetocaloric effect · Gas-atomization · Rare earth compounds · hydrogen liquefaction

1 Introduction

Magnetic refrigeration is a promising cooling technology for replacing conventional vapor compression refrigeration. It is

based on the magnetocaloric effect (MCE) of magnetic materials and has the advantages of high efficiency, energy saving, and environmentally friendliness [1, 2, 3, 4, 5, 6]. Among potential applications, there is an increasing interest in hydrogen liquefaction by magnetic refrigeration [7], because liquid hydrogen is one of the efficient form for transportation and storage in the so-called hydrogen society in which hydrogen is used as an energy carrier [8]. In order to establish the magnetic refrigeration technology for hydrogen liquefaction, much effort has been devoted to the search for new magnetic materials with a large MCE [12, 9, 10, 11] and the development of highly-efficient refrigeration systems using an active magnetic regenerators (AMR) cycle [13, 14, 15, 16].

On the other hand, the candidate materials should be processed into spheres for practical use in the AMR system [17, 18, 19]. A large surface area of spheres is desirable for getting a good heat exchange between spheres and a heat-exchanger fluid, which is important for better performance of an AMR system. The smaller particle size, the higher heat exchange efficiency, but the concomitant increase in pressure loss leads to poor performance. Considering the trade-off between the two, it is desirable that the particle diameter is on the order of submillimeter [20].

In 2020, the ferromagnetic material HoB₂ has been found to exhibit a giant MCE near the liquefaction temperature of hydrogen (20.3 K) [21]; The magnetic entropy change (ΔS_M) at a Curie temperature (T_C) of 15 K has a maximum value of 40.1 J kg⁻¹ K⁻¹ (0.35 J cm⁻³ K⁻¹) for a magnetic field change of 5 T, which is greater than those observed in any bulk materials that have been studied for magnetic hydrogen liquefiers. Due to such the ΔS_M and T_C , HoB₂ is expected to work as suitable magnetic refrigerants for hydrogen liquefaction. However, the material properties of this boride make it difficult to process it into the desired spherical shape. For instance, HoB₂ has a high melting point of 2350 °C compa-

Takafumi D. Yamamoto · Hiroyuki Takeya · Akiko T. Saito · Kensei Terashima · Pedro Baptista de Castro · Takenori Numazawa · Yoshihiko Takano

National Institute for Materials Science, Tsukuba, Ibaraki 305-0047, Japan

E-mail: YAMAMOTO.Takafumi@nims.go.jp

Pedro Baptista de Castro · Yoshihiko Takano

University of Tsukuba, Tsukuba, Ibaraki 305-8577, Japan

erable to those of ceramics. Accordingly, conventional atomization techniques [22] that melt and/or superheat a target material in a ceramic crucible cannot be used. Besides, the plasma rotating electrode process [23,24] is a non-contact type method to produce a high-purity spherical particles, but the brittle nature of HoB_2 hinders making an electrode and using it with high speed rotations during the processing.

In this study, we succeed in fabricating HoB_2 spherical particles for the first time by using an electrode induction melting gas atomization (EIGA) technique, in which the electrode rod of a material is melted without the use of the crucible. The resulting particles are evaluated in terms of morphology, phase confirmation, and various physical properties including magnetocaloric properties.

2 Experimental details

Figure 1 depicts the diagram of preparation process of HoB_2 spherical particles. The HoB_2 electrode rods were made by arc-melting in a water-cooled copper heath arc furnace. Stoichiometric amounts of Ho (3N) and B (3N) elements were arc-melted under an Ar-atmosphere. Each rod was flipped and melted several times for homogenizing the sample. The resulting electrode rods were 100-300 g in weight. In the present EIGA process, one end of HoB_2 electrode rod was fixed with a chuck in an Ar-atmosphere. The rod was immersed into an induction coil and inductively melted at the other end. The molten metal then freely fell through the orifice, atomized by jetting Ar-gas, and solidified into spheres. After the atomization, the collected powder was sieved into six fractions, $<100 \mu\text{m}$, $100\text{-}212 \mu\text{m}$, $212\text{-}355 \mu\text{m}$, $355\text{-}500 \mu\text{m}$, $500\text{-}710 \mu\text{m}$, and $>710 \mu\text{m}$, through a series of JIS Z 8801 standard sieves with a FRITSCH vibratory sieve shaker ANALYSETTE 3. The sieved powder consisted of spherical particles and off-round ones, so the former were separated from the latter by rolling them on a sloped belt conveyor.

Microstructural observation was carried out using a Hitachi SU-70 scanning electron microscope (SEM) operated at 20 kV. Powder X-ray diffraction (XRD) measurements were performed at room temperature by a Rigaku Mini-

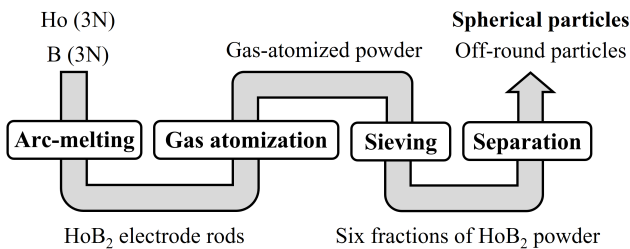


Fig. 1 (Color Online) The diagram of preparation process of HoB_2 spherical particles.

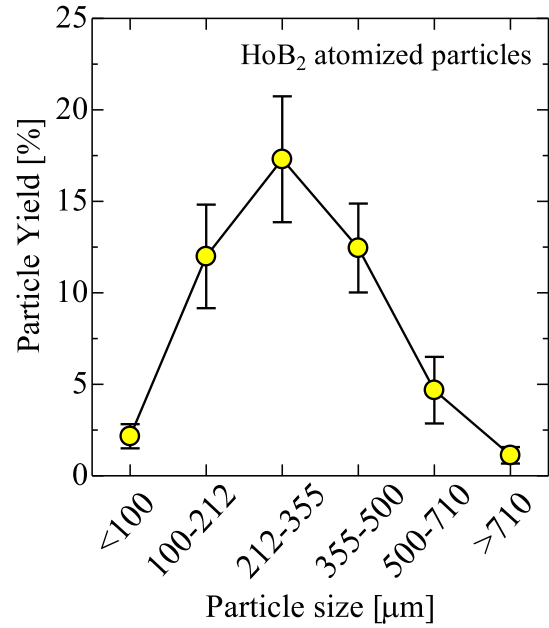


Fig. 2 (Color Online) Particle size distribution of HoB_2 spherical particles.

Flex600 diffractometer with Cu $K\alpha$ radiation. The temperature dependence of magnetization (M - T curves) at various magnetic fields ($\mu_0 H$) ranging from 0.01 to 5 T were measured between 2 and 50 K in field cooling processes by a Quantum Design SQUID magnetometer. The isothermal magnetization curves (M - H curves) were collected at 2 K between 0 and 5 T. The magnetic entropy change was evaluated from a series of the M - T curves according to a Maxwell's relation

$$\Delta S_M(T, \mu_0 \Delta H) = \mu_0 \int_0^H \left(\frac{\partial M}{\partial T} \right)_H dH, \quad (1)$$

where $\mu_0 \Delta H$ is the magnetic field change from zero to $\mu_0 H$. In the magnetization measurements, the bulk sample was formed into a rectangular shape with dimensions of $2.4 \times 0.5 \times 0.5 \text{ mm}^3$, and dozens of the spherical particles in contact with each other were arranged vertically long with the aspect ratio of about 2-4. The magnetic field was applied along the longitudinal directions of both the rectangular and the arranged spheres. The specific heat data at 0 T were measured by a thermal relaxation method with a Quantum Design PPMS.

3 Results and discussion

Figure 2 shows the particle size distribution for HoB_2 spherical particles. The gas atomization process was performed repeatedly, and the average values of the resulting yield are shown here. We find that the yield of the spherical particles has a significant value in the range from 100 to 710 μm , where the distribution patterns are centered around 212-355

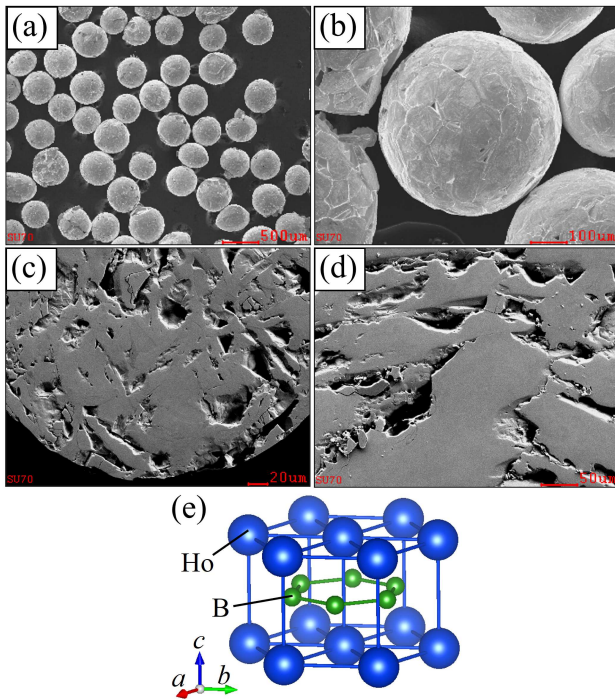


Fig. 3 (Color Online) (a) SEM image of surface and (b) its enlarged image for HoB₂ particles with 355-500 μm diameter. The cross-sectional SEM image of (c) the HoB₂ particles and (d) the HoB₂ electrode. (e) The crystal structure of HoB₂ with the space group of $P6/mmm$.

μm with the yield of 14-20wt% of the total melted electrode. The obtained particle size range is suitable for AMR systems. This may be due to the fact that the atomizing gas pressure in this study was set to 1.5-3.5 MPa, which is lower than the values used in conventional EIGA experiments for producing fine powder [25, 26, 27], in which the particle size is typically 100 μm or less [25, 26, 27, 28, 29].

Figure 3(a) shows a SEM image of surface for HoB₂ particles with 355-500 μm diameter. The majority of the particles are mostly spherical and has no satellites as is seen in other gas-atomized materials [29, 30, 31]. By using an image analysis software Image-J (National Institute of Health, US), the roundness of these particles is evaluated to be about 0.88. This quantity, defined as $4 \times (\text{Area}) / (\pi \times (\text{Major axis})^2)$, equals 1 for a circular object and less than 1 for an object that departs from circularity. The obtained value of the roundness guarantees the good sphericity of HoB₂ gas-atomized particles.

As shown in Fig. 3(b), however, the surface of each particle is not smooth but has a turtle shell-like structure. Moreover, a more complex inner structure with voids can be seen in Fig. 3(c). It should be noted that such internal voids do not result from the gas atomization process, because similar internal texture is observed in the HoB₂ electrode (Fig. 3(d)). These microstructures on the surface and inside can be attributed to the crystal structure of HoB₂. This diboride has

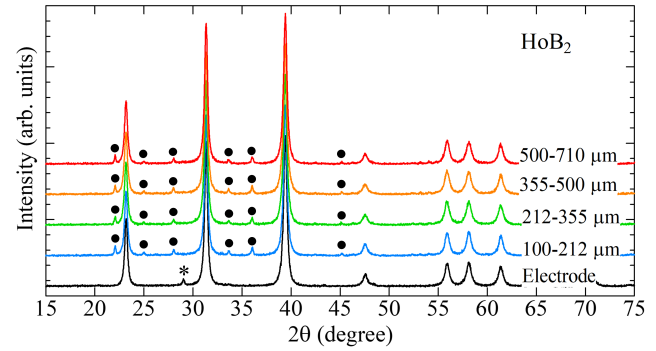


Fig. 4 (Color Online) Powder X-ray diffraction patterns of HoB₂ electrode and HoB₂ particles with various diameters from 100 to 710 μm . The marks indicate the Bragg peaks of Ho₂O₃ (*) and HoB₄ (●).

a layered structure with a hexagonal B-network as shown in Fig. 3(e), so the crystals are expected to grow while being oriented along the ab -plane. When the sample is solidified relatively quickly in the gas-atomization process and the arc-melting process, it is possible that the crystals are oriented inhomogeneously and consequently the microstructures are formed.

The powder XRD patterns shown in Fig. 4 confirm that both HoB₂ spherical particles and HoB₂ electrode have the main phase of the hexagonal HoB₂ with the space group of $P6/mmm$. The position and width of HoB₂ peaks are the same before and after atomizing, which suggests no change in crystallographic properties of HoB₂ phase by the atomization process. Furthermore, no differences in the peaks are found in all the atomized samples. Even though the solidification rate should depend on the particle diameter, it does not seem to affect the crystal structure of HoB₂. As an impurity phase, a tiny amount of Ho₂O₃ is found for the electrode while it disappears after atomizing. Instead, a bit trace of HoB₄ is observed in all the atomized particles. HoB₂ is a peritectic system in which it decomposes into solid HoB₄ and a Ho-rich liquid phase at 2200 °C before completely melted at 2350 °C [32]. Thus, HoB₄ probably appeared when the HoB₂ electrode was melted in the atomization process. Nevertheless, there are no other impurities, implying that it is free from contamination during the processing.

Now let us investigate the physical properties of the HoB₂ atomized particles. Figure 5(a) shows the M - T curves at 0.01 T in field cooling processes. Here the data for the electrode is scaled by 0.65 for visibility. In both the electrode and all the particles with different diameters, the magnetization rapidly increases as the temperature decreases toward 15 K, which is indicative of a ferromagnetic transition. The Curie temperature T_C , defined as a peak temperature of dM/dT , is evaluated to be 15.5 K for all the samples (see the inset of Fig. 5(a)). Furthermore, all the M - T curves exhibit a kink anomaly around 11 K, which is associated with the

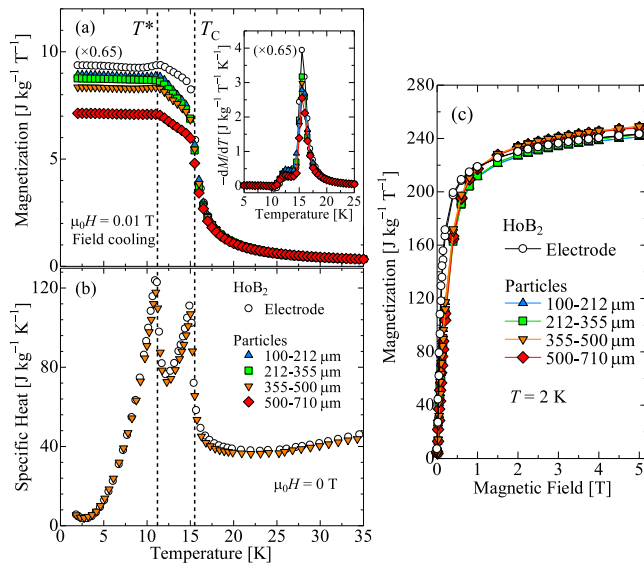


Fig. 5 (Color Online) Temperature dependence of (a) magnetization at 0.01 T and (b) specific heat at 0 T in HoB₂ electrode and HoB₂ particles. (c) Isothermal magnetization curves at 2 K. The inset in (a) depicts the temperature derivative of magnetization dM/dT at 0.01 T.

spin-reorientation phenomenon [33]. The kink temperature, named by T^* , does not change before and after the atomization process. As shown in Fig. 5(b), the well-defined peaks in specific heat at 0 T are observed around T_C and T^* , meaning that clear phase transitions take place at each temperature. These peaks in the HoB₂ particles are as sharp as those in the electrode. In addition, the M - H curves at 2 K for all the samples have a similar magnetic field dependence and quantitatively agree with each other in high magnetic fields (Fig. 5(c)). All these results suggest that the HoB₂ spherical particles are homogeneous and of good quality comparable to the bulk counterpart.

The disagreement in M - H curves below 1 T between the electrode and the particles should reflect the extrinsic demagnetization effect: The lower aspect ratio of the arranged particles can result in a larger demagnetization field. The difference between the M - T curves is also probably due to that of the aspect ratio. Accordingly, we conclude that there is no intrinsic dependence of magnetic properties on the particle diameter. In the gas-atomization process, the quenching effect on atomized particles is expected, and the cooling time of atomized particles can vary by diameter. No diameter dependence implies that the quenching effect has no impacts on the magnetic properties of HoB₂. This is consistent with no differences in physical properties between the electrode and the particles. Note that it is difficult at this stage to discuss the relationship of the quenching effect with the physical properties in depth, because the nature of HoB₂ itself has not been clarified.

It should be also discussed whether the impurity HoB₄ affects the physical properties of the HoB₂ particles. This

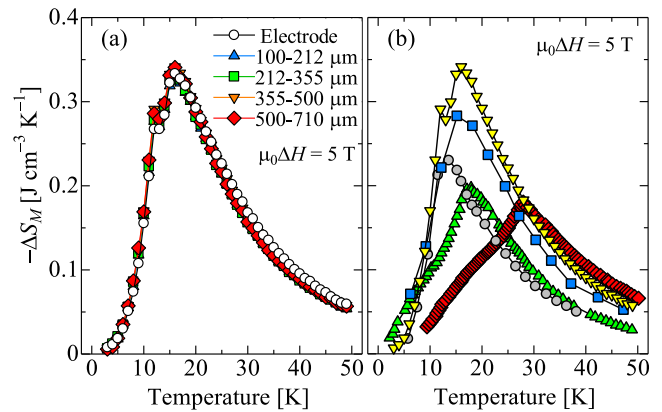


Fig. 6 (Color Online) (a) Magnetic entropy change for $\mu_0 \Delta H = 5$ T in HoB₂ particles and HoB₂ electrode. (b) The comparison of the HoB₂ particles with 355-500 μm diameter (∇) and other promising magnetocaloric materials: ErAl₂ (\circ) [38], HoN (\square) [39], EuS (\triangle) [40], and HoAl₂ (\diamond) [41].

tetraboride is known to exhibit two antiferromagnetic-like transitions at 7.1 K and 5.7 K, at which the magnetization shows a kink or drop and the specific heat shows sharp peaks [34,35]. As is evident in Figs. 5 (a) and 5 (b), no such anomalies are found in the data for the HoB₂ particles. Thus, it is likely that HoB₄ with a small amount has no influence on the final physical properties of HoB₂. This is true for a small amount of Ho₂O₃, which has an antiferromagnetic transition temperature of 2 K [36].

Finally, we will evaluate the magnetocaloric properties of the HoB₂ atomized particles. Figure 6(a) shows the magnetic entropy change ΔS_M for $\mu_0 \Delta H = 5$ T in the spherical particles and the electrode. Here we take J cm⁻³ K⁻¹ as the units of ΔS_M as this unit is meaningful from an engineering point of view [4]. Besides, it has shown that the demagnetization effect does not seriously affect the evaluation of ΔS_M for the large $\mu_0 \Delta H$ [37]. The ΔS_M is qualitatively and quantitatively the same between all the spherical particles and the bulk counterpart: It peaks at T_C and T^* and takes the maximum value of about 0.34 J cm⁻³ K⁻¹ at T_C . These results are almost consistent with those in our previous work [21]. Therefore, it is found that HoB₂ spherical particles prepared in this study have the same magnetocaloric properties as bulk material. Furthermore, we would like to compare here HoB₂ with other promising magnetocaloric materials that have similar magnetic transition temperatures. It can be seen from Fig. 6(b) that the ΔS_M of HoB₂ is not only large in peak value, but also has the advantage of keeping a large value up to high temperatures. It is worth noting that the values of ΔS_M in HoB₂ are comparable to those in HoAl₂ even at above 30 K. This feature of HoB₂ is attractive as magnetic refrigerants in that it is able to work over a wide temperature range.

4 Conclusion

We have succeeded in producing the spherical particles of a giant magnetocaloric compound HoB₂ by the electrode induction melting gas atomization technique. The obtained particle size range is suitable for AMR systems: it ranges from 100 to 710 μm centered at 212-355 μm with the highest yield of 15-25wt% of total melted electrode. The resulting particles have almost perfect spherical shape and no contamination during the processing. Furthermore, they have the characteristic microstructures on the surface and inside, which may originate from the crystallographic nature of HoB₂. The physical properties of the spheres are quite similar to those of the bulk counterpart, in which the sharp magnetic transitions and the giant magnetic entropy change are observed. All the results suggest that the gas-atomized HoB₂ particles have good potential as magnetic refrigerants for use in magnetic hydrogen liquefiers.

Not limited to HoB₂, magnetocaloric materials are often high melting point materials, which may hinder processing them into particles by conventional atomization methods. Our experimental results have demonstrated that the present atomization process is a viable route to fabricate spherical particles, even for the materials with melting points above 2000 °C. This fact would encourage the production of particles for various magnetocaloric compounds, which makes a significant contribution for developing magnetic refrigeration systems.

Acknowledgements This work was supported by JST-Mirai Program Grant Number JPMJMI18A3, Japan.

Compliance with ethical standards

Conflict of interest

The authors declare that they have no conflict of interest.

References

- Zimm C, Jastrab A, Sternberg A, Pecharsky V, Gschneidner Jr K, Osborne M, Anderson I (1998) Description and performance of a near-room temperature magnetic refrigerator. *Adv Cryog Eng* 43: 1759-1766.
- Tegus O, Brück E, Buschow KHJ, de Boer FR (2002) Transition-metal-based magnetic refrigerants for room-temperature applications. *Nature* 415: 150-152.
- Brück E (2005) Developments in magnetocaloric refrigeration. *J Phys D: Appl Phys* 38: R381-R391.
- Gschneidner Jr KA, Pecharsky VK, Tsokol AO (2005) Recent developments in magnetocaloric materials. *Rep Prog Phys* 68: 1479-1539.
- Lyubina J (2017) Magnetocaloric materials for energy efficient cooling. *J Phys D: Appl Phys* 50, 053002.
- Franco V, Blázquez JS, Ipus JJ, Law JY, Moreno-Ramírez LM, Conde A (2018) Magnetocaloric effect: From materials research to refrigeration devices. *Prog Mater Sci* 93: 112-232.
- Numazawa T, Kamiya K, Utaki T, Matsumoto K (2014) Magnetic refrigerator for hydrogen liquefaction. *Cryogenics* 62: 185-192.
- Sherif SA, Zeytinoglu N, Veziroğlu TN (1997) Liquid hydrogen: Potential, problems, and a proposed research program. *Int J Hydrogen Energy* 22: 683-688.
- Li DX, Yamaura T, Nimori S, Homma Y, Honda F, Haga Y, Aoki D (2014) Large reversible magnetocaloric effect in ferromagnetic semiconductor EuS. *Solid State Commun* 193: 6-10.
- Matsumoto KT, Hiraoka K (2017) Magnetocaloric effect in Gd-based ferromagnet GdZn₂. *J Magn Magn Mater* 423: 318-320.
- Omote H, Watanabe S, Matsumoto K, Gilmudtinov I, Kiiamov A, Tayurskii D (2019) Magnetocaloric effect in single crystal GdTlO₃. *Cryogenics* 101: 58-62.
- Zhang H, Gimaev R, Kovalev B, Kamilov K, Zverev V, Tishin A (2019) Review on the materials and devices for magnetic refrigeration in the temperature range of nitrogen and hydrogen liquefaction. *Phys B: Condens Matter* 558: 65-73.
- Kamiya K, Takahashi H, Numazawa T, Nozawa H, Yanagitani Y (2007) Hydrogen Liquefaction by Magnetic Refrigeration. *Cryocooler* 14: 637-644.
- Utaki T, Kamiya K, Nakagawa T, Yamamoto TA, Numazawa T (2007) Research on a Magnetic Refrigeration Cycle for Hydrogen Liquefaction. *Cryocooler* 14: 645-652.
- Matsumoto K, Kondo T, Yoshioka S, Kamiya K, Numazawa T (2009) Magnetic refrigerator for hydrogen liquefaction. *J Phys: Conf Ser* 150, 012028.
- Kim Y, Park I, Jeong S, (2013) Experimental investigation of two-stage active magnetic regenerative refrigerator operating between 77 K and 20 K. *Cryogenics* 57: 113-121.
- Yu B, Liu M, Egolf PW, Kitanovski A (2010) A review of magnetic refrigerator and heat pump prototypes. *Int J Ref* 33: 1029-1060.
- Nielsen KK, Tušek J, Engelbrecht K, Schopfer S, Kitanovski A, Bahl CRH, Smith A, Pryds N, Peredos A (2011) Review on numerical modeling of active magnetic regenerators for room temperature applications. *Int J Ref* 34: 603-616.
- Tušek J, Kitanovski A, Poredoš A (2013) Geometrical optimization of packed-bed and parallel-plate active magnetic regenerators. *Int J Ref* 36: 1456-1464.
- Barclay JA, Sarangi S (1984) Selection of Regenerator Geometry for Magnetic Refrigerator Applications. *Cryog Proc Equip* 51, 1.
- Castro PB, Terashima K, Yamamoto TD, Hou Z, Iwasaki S, Matsumoto R, Adachi S, Saito Y, Song P, Takeya H, Takano Y (2020) Machine-learning-guided discovery of the gigantic magnetocaloric effect in HoB₂ near the hydrogen liquefaction temperature. *NPG Asia Materials* 12, 35.
- Antony LVM, Reddy RG (2003) Processes for Production of High-Purity Metal Powders. *JOM* 55: 14-18.
- Miller SA, Nicholson JD, Gschneider Jr KA, Pecharsky AO, Pecharsky VK (2001) Manufacturing Considerations for Rare Earth Powders Used in Cryocooler and Magnetic Refrigerator Applications. *Cryocooler* 11: 449-455.
- Fujita A, Koiwai S, Fujieda S, Fukamichi K, Kobayashi T, Tsuji H, Kaji S, Saito AT (2007) Active Magnetic Regeneration Behavior of Spherical Hydrogenerated La(Fe_{0.86}Si_{0.14})₁₃ Fabricated by Rotating Electrode Process. *J J Appl Phys* 46: L154-L156.
- Franz H, Plochl L, Schimansky FP (2008) Recent Advances of Titanium Alloy Powder Production by Ceramic-free Inert Gas Atomization. *Titanium 2008 International Titanium Association*, 198.
- Xie B, Fan YZ, Miao QD (2019) Study on the process of TC4 powders prepared by electrode induction melting gas atomization for laser 3D printing. *IOP Conf Ser: Mater Sci Eng* 668, 012008.

27. Sun X, Yuan L, Wang L, Cheng L (2019) Study on the Formability of 3D Printed TC4 Alloy Powder by EIGA. *IOP Conf Ser: Mater Sci Eng* 493, 012134.
28. Feng S, Xia M, Ge CC (2017) Consecutive induction melting of nickel-based super alloy in electrode induction gas atomization. *Chin Phys B* 26, 060201.
29. Guo RP, Xu L, Zong BYP, Yang R (2017) Characterization of Pre-alloyed Ti-6Al-4V Powders from EIGA and PREP Process and Mechanical Properties of HIPed Powder Compacts. *Acta Metall Sin (Engl Lett)* 30: 735-744.
30. Mayer C, Dubrez A, Pierronnet M, Vikner P (2014) Towards the large scale production of $(La_{1-z}Ce_z)(Fe_{1-x-y}Mn_ySi_x)_{13}H_n$ products for room temperature refrigeration. *Phys Status Solidi C* 11: 1059-1063.
31. Osborne MG, Anderson IE, Gschneidner Jr KA (1994) Centrifugal atomization of neodymium and Er_3Ni regenerator particulate. *Adv Cryog Eng* 40: 631-638.
32. Liao PK, Spear KE (1990) B-Ho (Boron-Holmium). *Binary Alloy Phase Diagrams*, II Ed. 1k Ed. T. B. Massalski: 491-493.
33. Terada N, Terashima K, Castro PB, Colin CV, Mamiya H, Yamamoto TD, Takeya H, Sakai O, Takano Y, Kitazawa H (2020) Relationship between magnetic ordering and gigantic magnetocaloric effect in HoB_2 studied by neutron diffraction experiment. *Phys Rev B* 102, 094435.
34. Fisk Z, Maple M B, Johnston D C, Woolf L D (1981) Multiple phase transitions in rare earth tetraborides at low temperature. *Solid State Commn* 39, 1189-1192.
35. Kim J Y, Cho B K, Han S H (2009) Anisotropic magnetic phase diagrams of HoB_4 single crystal. *J Appl Phys* 105, 07E116.
36. Boutahar A, Moubah R, Hlil EK, Lassri H, Lorenzo E (2017) Large reversible magnetocaloric effect in antiferromagnetic Ho_2O_3 powders. *Sci Rep* 7, 13904.
37. Bez HN, Yibole H, Pathak A, Mudryk Y, Pecharsky VK (2018) Best practices in evaluation of the magnetocaloric effect from bulk magnetization measurements. *J Magn Magn Mater* 458: 301-309.
38. Pecharsky VK, Gschneidner KA (1999) Magnetocaloric effect from indirect measurements: Magnetization and heat capacity. *J Appl Phys* 86, 565.
39. Yamamoto TA, Nakagawa T, Sako K, Arakawa T, Nitani H (2004) Magnetocaloric effect of rare earth mono-nitrides, TbN and HoN. *J Alloys Compd* 376, 17-22.
40. Matsumoto K, Li L, Hirai S, Nakamura E, Murayama D, Ura Y, Abe S (2016) Large magnetocaloric effect in sintered ferromagnetic EuS. *Cryogenics* 79, 45-48.
41. Hashimoto T, Kuzuhara T, Sahashi M, Inomata K, Tomokiyo A, Yayama H (1987) New application of complex magnetic materials to the magnetic refrigerant in an Ericsson magnetic refrigerator. *J Appl Phys* 62, 3873.